Mechanism of Electric Power Generation from Ionic Droplet Motion on Polymer Supported Graphene

Shanshan Yang,[†,‡] Yudan Su,[†,‡] Ying Xu,[†] Qiong Wu,[†] Yuanbo Zhang,[†,§] Markus B. Raschke,[#] Mengxin Ren,[∥] Yan Chen,[⊥] Jianlu Wang,[⊥] Wanlin Guo,[¶] Y. Ron Shen,[⊗] and Chuanshan Tian*,[†,§]

[†]Department of Physics, State Key Laboratory of Surface Physics and Key Laboratory of Micro- and Nano-Photonic Structures (MOE), Fudan University, Shanghai 200433, China

[§]Collaborative Innovation Center of Advanced Microstructures, Nanjing 210093, China

[#]Department of Physics, Department of Chemistry, and JILA, University of Colorado, Boulder, Colorado 80309, United States

[∥]School of Physics and TEDA Applied Physics Institute, Nankai University, Tianjin 300071, China

[⊥]National Laboratory for Infrared Physics, Shanghai Institute of Technical Physics, Chinese Academy of Sciences, Shanghai 200083, China

[¶]Institute of Nanoscience, Nanjing University of Aeronautics and Astronautics, Nanjing 210016, China

[⊗]Department of Physics, University of California, Berkeley, Berkeley, California 94720, United States

S *Supporting Information*

ABSTRACT: Graphene-based electric power generation that converts mechanical energy of flow of ionic droplets over the device surface into electricity has emerged as a promising candidate for blue-energy network. Yet the lack of a microscopic understanding of the underlying mechanism has prevented ability to optimize and control the performance of such devices. This requires information on interfacial structure and charging behavior at the molecular level. Here, we use sum-frequency vibrational spectroscopy to study the roles of solvated ions, graphene, surface moiety on substrate and water molecules at the aqueous solution/graphene/polymer interface. We discover that the surface dipole layer of the neutral polymer is responsible for ion attraction toward and adsorption at the graphene surface that leads to electricity generation in graphene. Graphene itself does not attract ions and only acts as a conducting sheet for the induced carrier transport. Replacing the polymer by an organic ferroelectric substrate could allow switching of the electricity generation with long durability. Our microscopic understanding of the electricity generation process paves the way for the rational design of scalable and more efficient droplet-motion-based energy transducer devices.
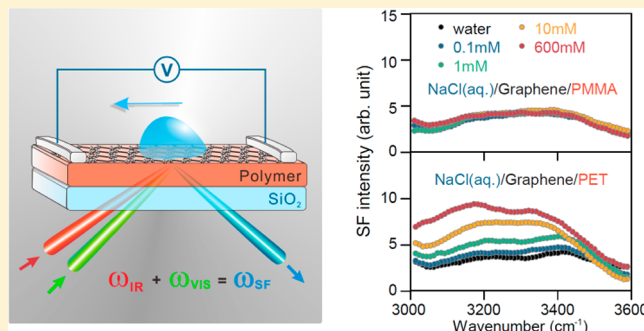
■ INTRODUCTION

The graphene−electrolyte interface has been demonstrated to exhibit promising attributes as a platform for a range of energy devices, such as solar cells,[1] supercapacitors,[2] and lithium-ion batteries.[3] Notably, a prototype of a novel graphene-based electric generator has recently been invented using a graphene−liquid interface to convert mechanical energy of moving ionic droplets to electric energy, offering an attractive new scheme for scalable electric power generation.[4−6] In such a device, droplets or waves of an ionic solution moving across graphene supported by an appropriate substrate generate a current in the graphene layer along or opposite to the flow direction.[4−12] More recently, such effect was observed at the aqueous interface with a polymer coated insulator−semiconductor structure.[13] Macroscopically, the governing mechanism of such electrokinetic phenomena can be explained by a drawing potential model.[5] It suggests that selective ions from

the solution can adsorb at the solid/solution interface and form a pseudocapacitor with the solid. As an ionic droplet moves along a graphene surface, ions that tend to adsorb on the interface are attracted toward the advancing front (charging of the pseudocapacitor) or repelled from the receding edge (discharging of the pseudocapacitor). Concurrently, oppositely charged carriers in graphene are attracted to the advancing and receding edge, resulting in a current flow in the graphene layer. Therefore, how effectively the ions can be attracted to the interface should determine the efficiency of electricity generation. At the microscopic scale, however, there are still arguments on the underlying mechanism that attracts ions to the solution/graphene interface.[5,9,10,14,15] This current lack of microscopic understanding hinders our ability to
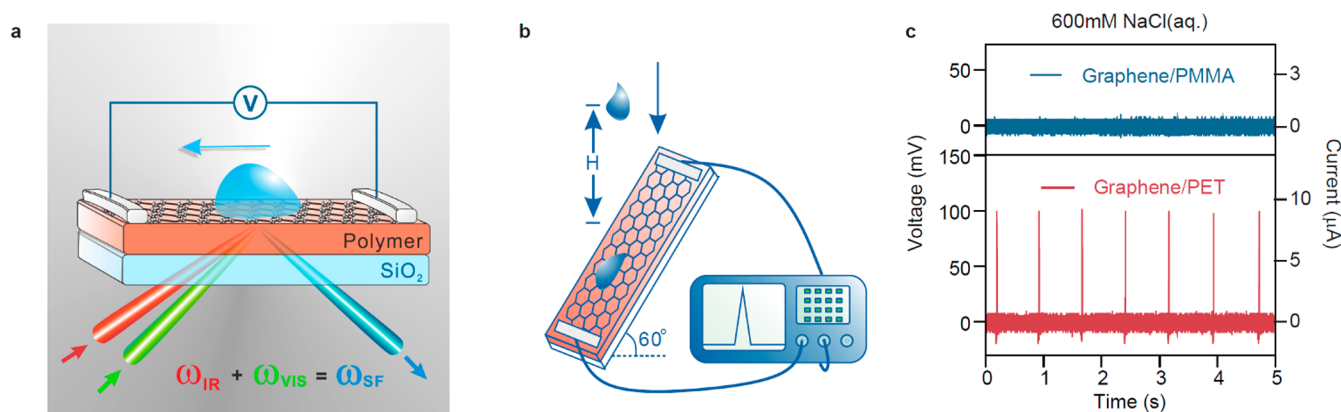
Figure 1. Electric voltage generation in polymer supported monolayer graphene device. (a) Experimental arrangement for electricity generation and SFVS measurements on a device consisting of a graphene/polymer film on a SiO$_2$ plate. (b) Cartoon describing the measurement of voltage generation by a falling aqueous droplet rolling on the graphene/polymer. (c) Left Y, oscilloscope traces showing presence and absence of voltage spikes generated from graphene/PET (red) and graphene/PMMA (blue, offset for clarity), respectively. Right Y, the generated current in graphene. The droplets were from a 600 mM NaCl aqueous solution.

optimize and control the performance of such graphene-based energy transducers. Moreover, the microscopic origin for ion adsorption at liquid/graphene interface is of great importance for graphene electrochemical device in general.

Most work to date has been focused on polymer-supported graphene devices. No consensus has been reached on the fundamental question of how the interface attracts the electrolyte ions to graphene surface. Several mechanisms have been proposed. Based on macroscopic experiments and calculations, some suggest that cations (Na$^+$) from electrolytic solution would preferentially adsorb on graphene.[5,14−20] Others postulate that a polymer substrate could be precharged by various means during sample preparation, for example, through friction before transferring of graphene on it,[9] or through piezoelectric effect;[12] the precharged polymer could attract ions from solution to graphene since the field screening effect by the monolayer graphene is weak.[21] To optimize such devices, it is imperative to pinpoint the mechanism on how solvated ions are drawn toward the interface and learn about the relevant parameters. This requires a molecular-level interfacial study of the device, and SFVS is known to be a unique analytical tool for liquid/solid interfaces.[22] Briefly, surface-specific SFVS is usually carried out by overlapping an infrared pulse (with a tunable frequency ω_{IR}) and a visible pulse (at ω_{vis}) at an interface and detecting the sum-frequency output in the reflected direction. As a second-order process, sum-frequency generation is forbidden in centrosymmetric media, but necessarily allowed at an interface where the inversion symmetry is broken. An effective surface nonlinearity, $\chi^{(2)}_{S,eff}(\omega = \omega_{vis} + \omega_{IR})$, can be used to describe the SF surface response, and is resonantly enhanced when ω_{IR} approaches surface resonances, yielding an SF vibrational spectrum for the interface. The dependence of the spectrum on the input and output polarizations provides information on the orientation of the species contributing to the resonances.

In this work, we report a SFVS study on polymer-supported graphene-based electricity generation devices. From sum-frequency vibrational spectra of polymer surfaces, solution/polymer interfaces, and solution/graphene/polymer interfaces, we find conclusively the following: Ions from the solution are not attracted by graphene, nor by a precharged surface; they are attracted to graphene/polymer, or polymer without graphene, by polar-ordered surface group with large dipole

moment of the polymer; the monolayer graphene appears as a weak screening layer for the dipole field and serves as a passive conductive path for the generated current; and the interaction between ions and the surface dipole layer is of short-range. We also present a general discussion on the parameters that may boost efficiency of the device. Our results provide a more comprehensive picture of electricity generation by the electrolytic solution/graphene/polymer devices that would help in future design of such devices for better efficiency and switchable operation.

RESULTS AND DISCUSSION

Electricity Generation by Moving Droplets on Graphene: The Role of Polymer Substrates. Figure 1a describes the device and the experimental arrangement in the present work. To avoid complication caused by possible contamination of graphene,[23] we developed a new method, different from the traditional one,[24] to lay graphene on polymer substrates, as described in the Experimental Section and Figure S1. Poly ethylene terephthalate (PET), poly methyl methacrylate (PMMA), and poly vinylidene fluoride (PVDF) were studied as substrates in our experiment.

To test electricity generation of the device, we adopted the falling droplet scheme (Figure 1b).[9] Successive drops of 600 mM NaCl solution, 5 mm in diameter, were let to roll down the graphene surface of the device, which was tilted 60° with respect to the horizontal. The initial speed of droplet on graphene was ~1 m/s that was controlled by the height H (Figure 1b and Section S8 in Supporting Information (SI)). Voltage pulses generated across the graphene by the droplets were recorded by an oscilloscope. The corresponding currents were calculated using the resistance of graphene and the load of the oscilloscope (Experimental Section). As shown in Figure 1c, positive voltage and current spikes (corresponding to positive ions attracted to the water/graphene interface) generated by sequential droplets on graphene/PET were readily observed, but were not detectable on graphene/PMMA. The results show clearly that the polymer substrates play dominant role in attracting ions to the water/graphene interface, and the PET substrate attracts Na$^+$ much more strongly than the PMMA substrate.

SFVS Probing of Surface Field Induced by Adsorbed Ions at the Interfaces. Sodium ion adsorption at the interface of water in contact with graphene/polymer can be explored by SFVS. It is known that a surface field at a water interface can reorient water molecules in the interfacial layer, leading to a spectral change that can be detected by SFVS.[25−31] The spectroscopic technique measures the OH stretch spectrum of the effective surface nonlinear susceptibility, $\chi^{(2)}_{S,eff}(\omega)$, of the interfacial water, which has the expression[32,33]

$$\chi^{(2)}_{S,eff}(\omega) = \chi^{(2)}_S + \int_{0^+}^{\infty} \chi^{(3)}_B E_{DC}(z) e^{i\Delta k_z z} dz \qquad (1)$$

Where $\chi^{(2)}_S$ denotes the contribution from a few monolayers of water molecules right at the interface, the integral describes the contribution from field-induced polarization of water molecules in the diffuse layer, $E_{DC}(z)$ is the distance dependent surface field along the surface normal, $\chi^{(3)}_B$ denotes the third-order nonlinear susceptibility of bulk water, and Δk_z is the phase mismatch of the SFVS process. The change of $\chi^{(2)}_{S,eff}(\omega)$, in particular $Im\chi^{(2)}_{S,eff}(\omega)$, directly reflects the change of $E_{DC}(z)$ in both magnitude and direction.

We conducted SFVS measurements on solution/polymer and solution/graphene/polymer interfaces. The existence of a surface field created by PET, but not by PMMA, can be seen from the spectral variation with increasing salt concentration in water. Ions in water can move toward the water interface in response to the surface field and modify the field. Figure 2a−d displays the spectra for the four aforementioned interfaces with different salt concentrations in water ranging from 0 to 600 mM. Within measurement error, the spectra of water/PMMA and water/graphene/PMMA are independent of the salt concentration (Figure 2a,b). This indicates that both interfaces are practically neutral. Obviously, ions do not come to the interface to alter the interfacial water structure. This is a clear manifestation that neither graphene nor PMMA attracts ions. The case of PET is different. The spectral intensity increases significantly with increase of salt concentration (Figure 2c,d), indicating that Na+ ions should have come to the interface to perturb the water structure. The spectrum of the water/graphene/PET interface at each salt concentration is slightly lower than that of the water/PET interface, indicating a weak screening effect of the monolayer graphene.

The positive ion attraction to graphene was speculated to be caused by pre-existing negative surface charges on the substrate before graphene was transferred onto it.[9] However, knowing that Na+ ions do not spontaneously adsorb on graphene, a negative surface charge layer on the polymer that attracts Na+ would have set up an electric double layer (EDL) with a negative surface field in the adjoining water and make $Im\chi^{(2)}_{S,eff}$ more positive. In contrast, a close look at the $Im\chi^{(2)}_{S,eff}$ spectra of the water/PET and water/graphene/PET interfaces for different salt concentrations in water reveals that they become more negative at higher salt concentration (Figure 2e,f).[34] This means that the surface field is positive and increases with salt concentration, orienting the interfacial water molecules with O → H more toward the bulk water, opposite to what is expected from a negatively precharged surface. This observation can only be explained by adsorption of Na+ ions at the interface creating a positive surface field.

Origin of Ion Adsorption at the Interface. With pre-existence of negative surface charges on PET out of the question, which is then the origin of Na+ ion adsorption at the interface? The surface of a polymer can often be polar with
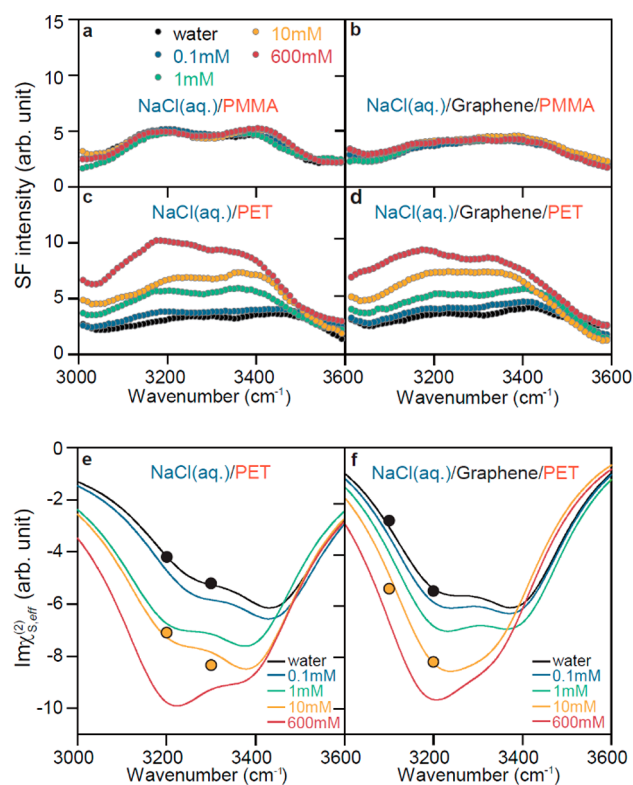
Figure 2. Bonded OH stretch SFVS spectra of interfacial water. (a and b) SF intensity spectra from the interfaces of NaCl(aq.)/PMMA and NaCl(aq.)/graphene/PMMA, respectively, for a set of different NaCl concentrations in the solution. The nearly identical spectra indicate no ion adsorption. In contrast, the SF intensity spectra from the interfaces of (c) NaCl(aq.)/PET and (d) NaCl(aq.)/graphene/PET increase with NaCl concentration. A slight field screening effect of graphene can be read from the lower spectral intensity in (d) in comparison to (c). The $Im\chi^{(2)}_{S,eff}$ spectra for (e) NaCl(aq.)/PET and (f) NaCl(aq.)/graphene/PET interfaces, deduced from the corresponding sum-frequency intensity spectra in panels c and d and discrete phase points in panels e and f measured directly by phase-sensitive SFVS, become increasingly negative with increasing NaCl concentration, indicating an increasing amount of Na+ ions adsorbed at the interface.

certain molecular groups polar-oriented at the surface. If the group has a strong dipole, the polymer should possess a strong surface dipole layer that can attract ions. SFVS can be used to probe the polar surface structure of a polymer buried under graphene. For PMMA with a chemical formula $[CH_2-C(CH_3)CO_2CH_3]_n$, it has been found that the side chains $-CO_2CH_3$ dominate on the surface with CH_3 projected out at 30° from the surface normal.[35] However, CH_3 has a very weak dipole ($\leq$1 D)[36] and accordingly, PMMA has a very weak surface dipole layer. In contrast, PET with $[C_8H_8(CO_2)_2]_n$ has the carbonyl groups (C=O) normally protruding out of the surface.[37] Because C=O has a very strong dipole ($\sim$2.7 D),[38] PET should have a strong dipole layer. Figure 3a shows the C=O stretch spectra of PMMA and PET surfaces covered by monolayer graphene, obtained by SFVS. The very prominent C=O peak at $\sim$1725 cm^{-1} for PET illustrates the strong polar ordering of C=O on the graphene/PET surface, while the undetectable C=O peak for graphene/PMMA indicates little polar ordering of C=O along the surface normal. The surface dipole layer of C=O with O pointing out on PET should play
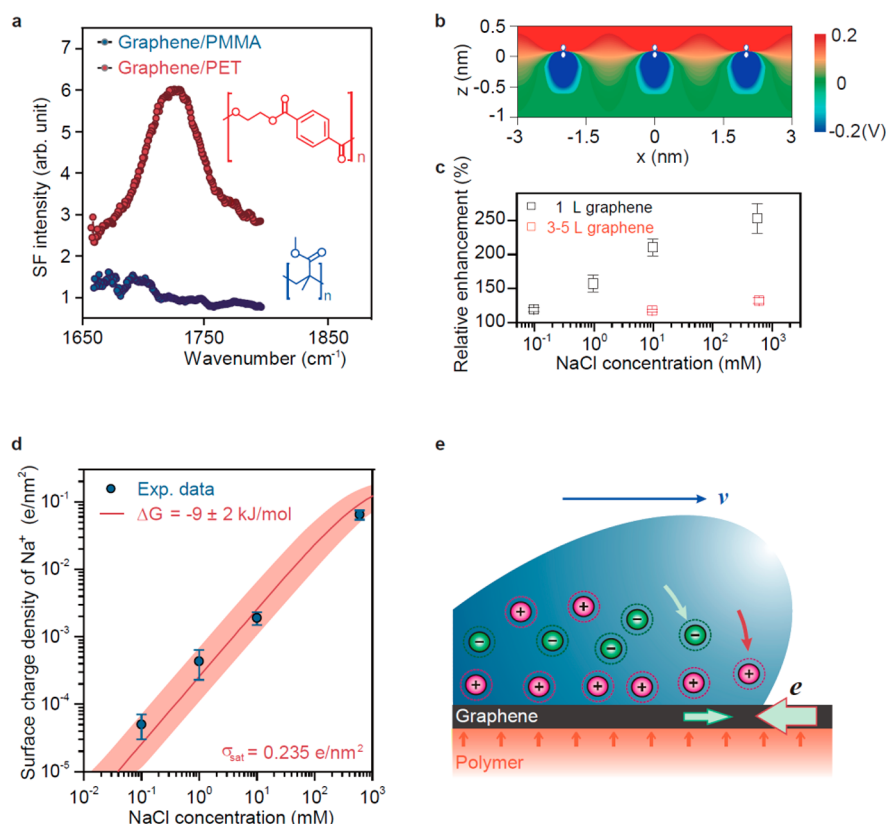
Figure 3. Origin of ion adsorption at water/graphene/PET interface. (a) Sum-frequency vibrational spectra showing the absence and presence of the C=O stretching mode at the graphene/PMMA and graphene/PET interfaces, respectively, denoting strong C=O polar ordering on the latter interface. (b) Calculated azimuthally isotropic electric potential in the $x-y$ plane generated by a square array of C=O dipoles with C → O pointing normally toward the solution. (c) Relative increase of sum-frequency intensities for monolayer and 3−5 layers of graphene/PET devices versus NaCl concentration, which are normalized against that of pure water. (d) Surface Na$^+$ density versus bulk NaCl concentration deduced from the Im$\chi_{S,eff}^{(2)}$ spectra using the Gouy−Chapman model. Fitting of the data points by a simple Langmuir isotherm, with the surface dipole density taken as the saturated ion density σ_{sat}, allows the deduction of the adsorption free energy ΔG. (e) Cartoon illustrates the motion of ions in solution and electrons in graphene toward the front edge of the droplet in response to an ionic droplet moving forward with velocity v.

dominant role in attraction of Na$^+$ to the water/graphene/PET interface.

Now the question is how a surface dipole layer can attract Na$^+$ from solution to adsorb on graphene/PET. It is well-known, from the continuum theory of electrostatics, that an infinite continuum of surface dipole layer has no field outside the layer. In reality, however, surface dipole forms a local potential well on top of each dipole that can trap ion.[39] For illustration, we plot, in Figure 3b, the calculated potential distribution in the $x-y$ plane created by a square array of C=O dipoles with C → O pointing normally toward the solution and a surface density equal to that of C=O on PET (Section S5 in Supporting Information). Positive ions adsorbed in the potential traps, now play the dominant role in setting up the positive surface field and the EDL in water at the interface. Because the surface dipole field is of short-range (Figure 3b), the screening effect of graphene can be appreciable. Accordingly, ion adsorption decreases significantly with increase of the graphene layer thickness. This is illustrated in Figure 3c, where it is seen that the increase of the sum-frequency signal with ion concentration, normalized against that of pure water, is much smaller for the 3−5 layer graphene/PET than for the monolayer graphene/PET. Note that, although the physical picture of ion-dipole interaction at the interface can be understood using the classic continuum dielectric theory, more quantitative analysis of the interaction

through graphene requires the knowledge of the effective dielectric constant that varies rapidly within nanometer-scale across the interface.

The adsorption energy of ions in the surface dipole traps is expected to be small for the C=O type surface dipoles. We can have an estimate on the adsorption energy from the observed spectral variation of interfacial water with different salt concentrations. As shown in eq 1, in the limit of low surface density of adsorbed ions (Na$^+$), only the second term on the right depends on the surface field $E_{DC}(z)$, which is generated by the adsorbed ions. With the help of the Gouy−Chapman model, we can relate $E_{DC}(z)$ to the surface ion density σ, and use it as an adjustable parameter to calculate the following:

$$\Delta \text{Im}\chi_{S,eff}^{(2)} = \text{Im}[\chi_{S,eff}^{(2)} - \chi_S^{(2)}] = \text{Im}\int_{0^+}^{\infty}\chi_B^{(3)}E_{DC}(z)e^{i\Delta k_z z}dz$$

and fit the measured $\Delta\text{Im}\chi_{S,eff}^{(2)}$ with known $\chi_B^{(3)}$ (Section S3 in Supporting Information). We can thus find σ for the different bulk ion concentrations specified in Figure 2. The data points are plotted in Figure 3d. We notice that the Na$^+$ ion surface density is very low, (0.062 e/nm^2 at the highest bulk concentration of 600 mM) and interactions between adsorbed ions can be neglected. Thus, the data can be reliably fitted by a simple Langmuir adsorption isotherm with the assumption that the saturated surface ion density, σ_{sat}, is equal to the C=O
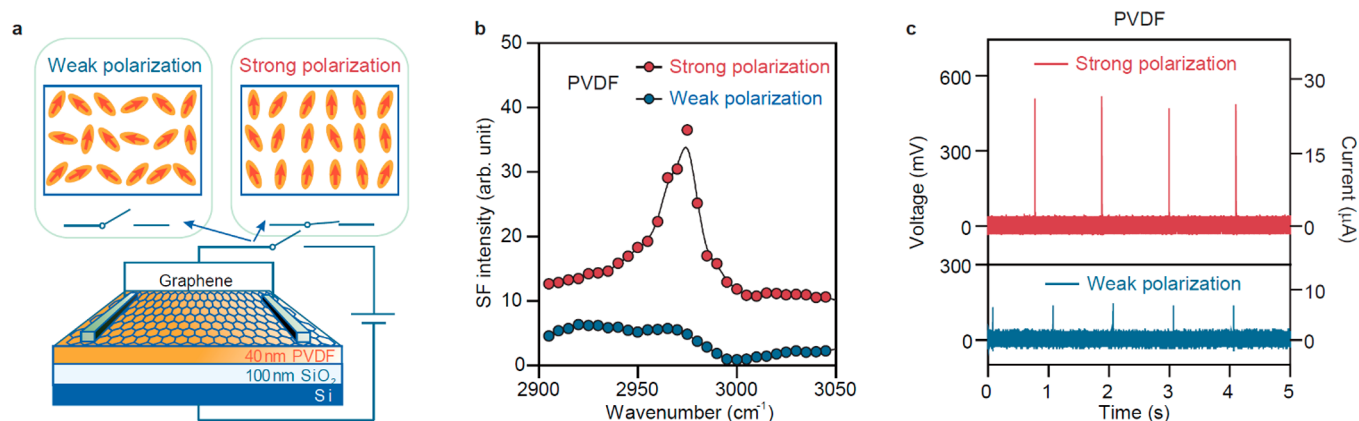
Figure 4. Gate-control switchable voltage generation with a ferroelectric polymer film. (a) Sketch of a device made of a graphene/PVDF/SiO$_2$/Si structure that can be gated across the layers by a bias voltage. The domain alignment of PVDF film along the surface normal can be controlled by the bias. (b) CH$_2$ stretching mode at 2975 cm^{-1} monitored by SFVS, indicating that PVDF is in the weakly polarized state (blue dots) or in the stronger polarized state (red dots). (c) Left Y, measured voltage spikes from the device showing that they are weak when PVDF is in the weakly polarized state and strongly enhanced when PVDF is in the stronger polarized state. Right Y, the deduced current flow across graphene from the resistances of 19.4 kΩ for poled and 20.6 kΩ for unpoled PVDF, respectively.

surface dipole density on PET (0.235/nm^2).[40] From the fit, we find an adsorption energy of $\Delta G = -9$ (± 2) kJ/mol (Section S4 in Supporting Information). This adsorption energy is indeed a few times smaller than the usual adsorption energy for molecular species adsorbed at an interface from solution.[41]

General Consideration for Optimization and Possible Gate Control on Electricity Generation. From what we learned about NaCl(aq.)/graphene/polymer interfaces, we can come up with the following general picture (Figure 3e) for electricity generation by such devices. Ions in water are attracted to graphene by the surface dipole layer, if present, of a polymer and tend to adsorb in the interfacial dipole potential traps. As a droplet of ionic solution moves on graphene, the fresh water/graphene interface is formed at the advancing water front. Sodium ions must rush over to the fresh interface. They increase the potential seen by electrons in graphene and attract them toward the fresh interface. Only in delayed action, the negative ions in the solution are dragged along by the positive ions and affect somewhat the current in graphene. This dynamic process constitutes the charging action. The opposite process occurs at the trailing edge of the droplet and constitutes the discharging action. As proposed previously,[5] electricity generation results from combined actions of charging and discharging. The above picture suggests that polymer substrates with a denser and stronger surface dipole layer should be more efficient in generating electricity. A quick estimate (Section S5 in Supporting Information) shows that the generated current can be increased by ~10-fold if dipole moment is doubled and its surface density is 4 times larger than that of C═O in PET. Besides, it is already known that larger droplet size, faster droplet velocity generally enhances the current generation, while electricity generation also varies with the type of ions in solution as the dynamics of ion motion depends on the size and charges of the ions.[5]

It may happen that the surface dipole layer of a polymer is so strong that ions adsorbing on it (or on graphene of the graphene/polymer film) do not desorb at the receding edge. However, such a surface would be easily passivated by counterions adsorbed from air. Accordingly, electricity generation efficiency of the device will be reduced. As a demonstration, we replace the PET substrate by a 1 mm z-cut

LiNbO$_3$ ferroelectric crystal. The LiNbO$_3$ surface generates a much stronger surface field than PET (Section S6 in Supporting Information), but exposing it to air rapidly decreases its surface potential. As a result, the voltage spikes generated by moving water droplets on graphene/LiNbO$_3$ are slightly larger than those in the PET case (Figure S5 in Supporting Information).

The LiNbO$_3$ case above suggests that the efficiency and durability of electricity generation of the device would be greatly improved with the use of ferroelectric films instead of surface-dipole films if surface passivation of ferroelectric films could be prevented. Because surface passivation comes from field-attracted ions, it is possible that they can be removed by switching off the ferroelectric polarization. This led us to the idea of constructing a switchable electricity generation device using a gate-controlled ferroelectric film. To demonstrate the idea, we used a thin film (40 nm) of β-polyvinylidene fluoride (PVDF, $-(-CF_2-CH_2-)_n-$) to replace the PET film in our device. β-PVDF is a well-known organic ferroelectric material with its domain consisting of ordered chains and the side groups ($-CF_2-CH_2-$).[42] The macroscopic ferroelectric polarization can be poled by an external electric field. In the device we studied (Figure 4a), the β-PVDF film was sandwiched between graphene and 100 nm silica grown on doped Si substrate. Graphene and Si were used as the gate electrodes for poling β-PVDF. The film was initially weakly polarized and was poled to become more strongly polarized by a gate voltage of 30 V on the two electrodes. The two polarization states were monitored by SFVS showing a strong methylene stretch peak in the latter but a very weak one in the former, as shown in Figure 4b. The generated voltage spikes, depicted in Figure 4c, were strong and weak, respectively, in the two cases. Reversing the applied voltage reversed the poling of PVDF and switched the polarity of electricity generation. (Notice that the output voltage difference here is not as large as that of SFVS signals. This is because the SFVS signal is from the whole poled 40 nm PVDF film, but only the first few layers of PVDF contribute to attraction of solvated ions toward the interface and the current generation in graphene. These results demonstrate that one could switch electricity generation on and off with gate voltages). In the off

state, ion adsorption at the interface is weak, and we should be able to clean the interface in situ by various means. Electricity generation of our device with PVDF was found to be 5 times stronger than the one with PET under the same working condition. Note that the device can be further improved through engineering of the PVDF film, for example, reduction of the switching voltage of the film.

CONCLUSIONS

In summary, graphene/polymer electricity generation devices are most promising because of their simplicity, flexibility, and scalability. Understanding of the underlying mechanism provides us with basic design concepts for possible improvement. Our finding that graphene does not attract ions and serves only as a conducting pathway for electricity generation suggests that it could be replaced by other conducting materials as long as their field-screening effect is weak. For better electricity generation efficiency of the solution/graphene/substrate devices, we suggest, for the substrate, use of polymers with stronger surface dipoles and denser dipole density, organic and inorganic ferroelectric films to improve ion attraction to the interface, as well as electrical gating to control and switch electricity generation.

EXPERIMENTAL SECTION

Preparation of Graphene Surface on PMMA or PET. In constructing the graphene/PMMA/fused silica device, PMMA was first spin-coated on graphene CVD-grown on a copper foil. A fused silica window was then pressed on PMMA and annealed at 150 °C for 15 min to have the window stick together with PMMA. The assembly was dipped into a 0.1 M $(NH_4)_2S_2O_8$ solution for 2 h to etch away the copper foil, followed by rinsing with deionized water, leaving the graphene surface uncontaminated. In the case of PET, a 10 μm PET film was heated to the glass phase, and a silica window was used to press it on graphene/copper foil. After cooling, the copper foil was etched away by the 0.1 M $(NH_4)_2S_2O_8$ solution. For the PVDF device, the traditional graphene transfer procedure was used.[24]

The metal electrical contacts on graphene were secured by silver epoxy and were covered by silica gel to prevent them from contacting the ionic solution.

The currents flow across graphene indicated by the right Y axis of Figure 1c were deduced from the resistance of graphene and the load of the oscilloscope. The resistance for the graphene on PET, PMMA, unpoled PVDF and poled PVDF was 11.4, 15.6, 20.6, 19.4 kΩ, respectively. The load of the oscilloscope was 1 MΩ.

Sum Frequency Vibrational Spectroscopy Measurement. For SF intensity, $|\chi_{S,eff}^{(2)}(\omega)|^2$, measurement, the SFVS setup was similar to those described earlier.[43] A picosecond Nd:YAG (Ekspla) laser with 20 Hz repetition rate was used to generate a visible beam at 532 nm and a tunable IR beam between 2800 and 3800 cm^{-1}. The two beams overlapping on the sample had pulse energies and beam spot diameters of 50 μJ and 1.5 mm and 50 μJ and 1.0 mm, respectively. The SF output was normalized to that from a z-cut quartz.

For phase-sensitive SFVS measurement,[44] the same input beams were used, but they propagated collinearly through a reference y-cut quartz plate and onto the sample at an incident angle of 45°. The SF signal generated from the y-cut quartz interfered with that from the sample in the reflected direction and provided the phase information about the SF output. $Im\chi_{S,eff}^{(2)}(\omega)$ was then deduced from the measured $|\chi_{S,eff}^{(2)}(\omega)|^2$ and the phase of $\chi_{S,eff}^{(2)}(\omega)$.

ASSOCIATED CONTENT

Ⓢ Supporting Information

The Supporting Information is available free of charge on the ACS Publications website at DOI: 10.1021/jacs.8b07778.

Sample preparation, sum frequency spectroscopy analysis, surface dipole layer modeling, electric signal measurement (PDF)

AUTHOR INFORMATION

Corresponding Author

*cstian@fudan.edu.cn.

ORCID Ⓘ

Markus B. Raschke: 0000-0003-2822-851X
Wanlin Guo: 0000-0001-9577-4532
Chuanshan Tian: 0000-0003-3341-1378

Author Contributions

‡Shanshan Yang and Yudan Su contributed equally.

Notes

The authors declare no competing financial interest.

REFERENCES

(1) Wang, X.; Zhi, L.; Mullen, K. *Nano Lett.* **2008**, *8*, 323.
(2) Hu, C. G.; Song, L.; Zhang, Z. P.; Chen, N.; Feng, Z. H.; Qu, L. T. *Energy Environ. Sci.* **2015**, *8*, 31.
(3) Yang, S.; Feng, X.; Ivanovici, S.; Mullen, K. *Angew. Chem., Int. Ed.* **2010**, *49*, 8408.
(4) Yin, J.; Zhang, Z.; Li, X.; Yu, J.; Zhou, J.; Chen, Y.; Guo, W. *Nat. Commun.* **2014**, *5*, 3582.
(5) Yin, J.; Li, X.; Yu, J.; Zhang, Z.; Zhou, J.; Guo, W. *Nat. Nanotechnol.* **2014**, *9*, 378.
(6) Wang, Z. L. *Nature* **2017**, *542*, 159.
(7) He, Y. J.; Lao, J. C.; Yang, T. T.; Li, X.; Zang, X. B.; Li, X. M.; Zhu, M.; Chen, Q.; Zhong, M. L.; Zhu, H. W. *Appl. Phys. Lett.* **2015**, *107*, 081605.
(8) Lao, J. C.; He, Y. J.; Li, X.; Wu, F. Z.; Yang, T. T.; Zhu, M.; Zhang, Y. Y.; Sun, P. Z.; Zhen, Z.; Cheng, B. C.; Zhu, H. W. *Nano Res.* **2015**, *8*, 2467.
(9) Kwak, S. S.; Lin, S.; Lee, J. H.; Ryu, H.; Kim, T. Y.; Zhong, H.; Chen, H.; Kim, S. W. *ACS Nano* **2016**, *10*, 7297.
(10) Tang, Q.; Wang, X.; Yang, P.; He, B. *Angew. Chem., Int. Ed.* **2016**, *55*, 5243.
(11) Tang, Q. W.; Yang, P. Z. *J. Mater. Chem. A* **2016**, *4*, 9730.
(12) Zhong, H. K.; Xia, J.; Wang, F. C.; Chen, H. S.; Wu, H. A.; Lin, S. S. *Adv. Funct. Mater.* **2017**, *27*, 1604226.
(13) Park, J.; Song, S.; Yang, Y.; Kwon, S. H.; Sim, E.; Kim, Y. S. *J. Am. Chem. Soc.* **2017**, *139*, 10968.
(14) Shi, G.; Liu, J.; Wang, C.; Song, B.; Tu, Y.; Hu, J.; Fang, H. *Sci. Rep.* **2013**, *3*, 3436.
(15) Tsai, S. J.; Yang, R. J. *Sci. Rep.* **2016**, *6*, 30731.
(16) Wang, X.; Zeng, Z.; Ahn, H.; Wang, G. *Appl. Phys. Lett.* **2009**, *95*, 183103.
(17) Ng, S. R.; Guo, C. X.; Li, C. M. *Electroanalysis* **2011**, *23*, 442.
(18) Umadevi, D.; Sastry, G. N. *J. Phys. Chem. Lett.* **2011**, *2*, 1572.
(19) Song, B.; Yang, J.; Zhao, J.; Fang, H. *Energy Environ. Sci.* **2011**, *4*, 1379.
(20) Mahadevi, A. S.; Sastry, G. N. *Chem. Rev.* **2013**, *113*, 2100.
(21) Rafiee, J.; Mi, X.; Gullapalli, H.; Thomas, A. V.; Yavari, F.; Shi, Y.; Ajayan, P. M.; Koratkar, N. A. *Nat. Mater.* **2012**, *11*, 217.
(22) Shen, Y. R. *Fundamentals of Sum-Frequency Spectroscopy*; Cambridge University Press: Cambridge, U. K., 2016.

(23) Su, Y.; Han, H. L.; Cai, Q.; Wu, Q.; Xie, M.; Chen, D.; Geng, B.; Zhang, Y.; Wang, F.; Shen, Y. R.; Tian, C. *Nano Lett.* **2015**, *15*, 6501.

(24) Li, X.; Cai, W.; An, J.; Kim, S.; Nah, J.; Yang, D.; Piner, R.; Velamakanni, A.; Jung, I.; Tutuc, E.; Banerjee, S. K.; Colombo, L.; Ruoff, R. S. *Science* **2009**, *324*, 1312.

(25) Gragson, D. E.; McCarty, B. M.; Richmond, G. L. *J. Am. Chem. Soc.* **1997**, *119*, 6144.

(26) Kim, J.; Kim, G.; Cremer, P. S. *Langmuir* **2001**, *17*, 7255.

(27) Ji, N.; Ostroverkhov, V.; Tian, C. S.; Shen, Y. R. *Phys. Rev. Lett.* **2008**, *100*, No. 096102, DOI: 10.1103/PhysRevLett.100.096102.

(28) Nihonyanagi, S.; Yamaguchi, S.; Tahara, T. *J. Chem. Phys.* **2009**, *130*, 204704.

(29) Sovago, M.; Vartiainen, E.; Bonn, M. *J. Chem. Phys.* **2009**, *131*, 161107.

(30) Chen, X.; Hua, W.; Huang, Z.; Allen, H. C. *J. Am. Chem. Soc.* **2010**, *132*, 11336.

(31) Ohno, P. E.; Saslow, S. A.; Wang, H. F.; Geiger, F. M.; Eisenthal, K. B. *Nat. Commun.* **2016**, *7*, 13587.

(32) Wen, Y. C.; Zha, S.; Liu, X.; Yang, S.; Guo, P.; Shi, G.; Fang, H.; Shen, Y. R.; Tian, C. *Phys. Rev. Lett.* **2016**, *116*, No. 016101, DOI: 10.1103/PhysRevLett.116.016101.

(33) Gonella, G.; Lutgebaucks, C.; de Beer, A. G. F.; Roke, S. *J. Phys. Chem. C* **2016**, *120*, 9165.

(34) Zhang, L.; Tian, C.; Waychunas, G. A.; Shen, Y. R. *J. Am. Chem. Soc.* **2008**, *130*, 7686.

(35) Wang, J.; Chen, C. Y.; Buck, S. M.; Chen, Z. *J. Phys. Chem. B* **2001**, *105*, 12118.

(36) Snyder, R. G. *J. Chem. Phys.* **1965**, *42*, 1744.

(37) Loch, C. L.; Ahn, D.; Chen, C. Y.; Wang, J.; Chen, Z. *Langmuir* **2004**, *20*, 5467.

(38) Roberts, J. D.; Caserio, M. C. *Basic Principles of Organic Chemistry*; W. A. Benjamin, Inc.: Menlo Park, CA, 1977.

(39) Cherepanov, D. A.; Feniouk, B. A.; Junge, W.; Mulkidjanian, A. Y. *Biophys. J.* **2003**, *85*, 1307.

(40) Chen, W.; McCarthy, T. J. *Macromolecules* **1998**, *31*, 3648.

(41) Tian, C. S.; Shen, Y. R. *Proc. Natl. Acad. Sci. U. S. A.* **2009**, *106*, 15148.

(42) Bune, A. V.; Fridkin, V. M.; Ducharme, S.; Blinov, L. M.; Palto, S. P.; Sorokin, A. V.; Yudin, S. G.; Zlatkin, A. *Nature* **1998**, *391*, 874.

(43) Xu, H. J.; Zhang, D. H.; Hu, J.; Tian, C. S.; Shen, Y. R. *J. Phys. Chem. A* **2015**, *119*, 4573.

(44) Sun, S. M.; Liang, R. D.; Xu, X. F.; Zhu, H. Y.; Shen, Y. R.; Tian, C. S. *J. Chem. Phys.* **2016**, *144*, 244711.